Microchimica Acta (2018) 185: 455
https://doi.org/10.1007/s00604-018-2984-2

ORIGINAL PAPER

Electrochemical sandwich immunoassay for *Escherichia coli* O157:H7 based on the use of magnetic nanoparticles and graphene functionalized with electrocatalytically active Au@Pt core/shell nanoparticles

Fanjun Zhu[1] · Guangying Zhao[1] · Wenchao Dou[1]

Received: 19 May 2018 / Accepted: 29 August 2018 / Published online: 13 September 2018

Abstract

A highly sensitive electrochemical sandwich immunoassay is described for determination of *Escherichia coli* O157:H7 (*E. coli* O157:H7). Silica coated magnetite nanoparticles (Fe_3O_4) were modified with primary antibody to capture *E. coli* O157:H7. Gold-platinum core/shell nanoparticles (Au@Pt NPs) with different Pt shell thicknesses were prepared via changing the molar ratio of H_2PtCl_6 to $HAuCl_4$ in the precursor solution. The optimized Au@Pt NPs exhibit enhanced activity in the electrocatalytic reduction of hydrogen peroxide (H_2O_2). The Au@Pt NPs were modified with graphene that was functionalized with Neutral Red, and then used as an electrochemical label for secondary antibodies and horseradish peroxidase (HRP). The sandwich immunocomplexes were magnetically absorbed on a 4-channel screen printed carbon electrode. Due to the catalysis of the Au@Pt NPs and HRP, the signal is strongly amplified in the presence of H_2O_2 when using thionine as the electron mediator. Under optimal conditions, the immunoassay has a linear response in the 4.0×10^2 to 4.0×10^8 CFU·mL^{-1} concentration range, with a limit of detection of 91 CFU·mL^{-1} (at an S/N ratio of 3).

Keywords Bimetallic nanoparticles · Screen printed carbon electrode · Horseradish peroxidase · Hydrogen peroxide · Gold-platinum core/shell nanoparticles · Reduced graphene oxide · Signal amplification · Bacteria · Nanomaterial · Food safety

Introduction

Escherichia coli O157:H7 (*E. coli* O157:H7), a gram-negative rod-shaped bacterium, is reported as the one of the causes linked to hemolytic uremic syndrome (HUS) in young and immuno-compromised individuals [1]. It has emerged as an enteric and highly infective food and water borne pathogen posing a tremendous challenge to public health [2]. As a result, it is important to develop methods for sensitive, reliable, and rapid detection of *E. coli* O157:H7. Compared with the other methods such as standard plate count [3], enzyme linked immunosorbent assay (ELISA) [4, 5] and hybridization assays [6–8], electrochemical immunoassays have attracted considerable attention in immunochemical field. Electrochemical immunoassays has intrinsic advantages such as rapid response, simple instrumentation and high specificity [9–11]. As early quality evaluation of daily food, it requires highly sensitive electrochemical immunoassay to accurately determine *E. coli* O157:H7 at low levels. Therefore, signal amplification is crucial for obtaining low detection limit and high sensitivity in electrochemical immunoassay.

With the development of nanoscience and nanotechnology, a variety of nanomaterials have enabled significant improvement in the analytical performance of electrochemical

Highlights
- The catalytic activity of Au@Pt core/shell nanoparticle with different Pt shell thickness was studied to increase the sensitivity.
- Using rGO-NR-Au@Pt-Ab_2-HRP as signal tag to amplify signal.
- Fe_3O_4@SiO_2-Ab_2 was used as capture probe for enriching and separating *E. coli* O157:H7.
- A sensitive sandwich-type electrochemical immunoassay for *Escherichia coli* O157: H7 was designed.

Electronic supplementary material The online version of this article (https://doi.org/10.1007/s00604-018-2984-2) contains supplementary material, which is available to authorized users.

✉ Wenchao Dou
wdou@zjsu.edu.cn

[1] Food Safety Key Laboratory of Zhejiang Province, College of Food Science and Biotechnology, Zhejiang Gongshang University, Hangzhou 310018, China

immunoassays [12]. Such as reduced graphene oxide (rGO), Fe_3O_4 magnetic nanoparticles (MNPs) and bimetallic nanoparticles. rGO has attracted much attention in electrochemical immunoassay for its unique electronic properties, large specific surface area, and excellent mechanical properties [13, 14]. But it is easily forms irreversible agglomerate in water. As a consequence, it is necessary to adopt appropriate measures to improve the performance of rGO before it is applied in the immunoassays. MNPs, possess an excellent superparamagnetic property and can be readily separated from reaction mixtures with an external magnet. After they are coated with silica (denoted as $Fe_3O_4@SiO_2$), it is ideal for them to be applied in bioanalysis. After introducing functional groups such as amine and carboxyl [15], $Fe_3O_4@SiO_2$ are also easy to modify with biomolecule. Bimetallic nanoparticles composed of two different metal elements have also received widespread attention especially in the field of electrochemical immunoassays. They often show improved catalytic performance than their monometallic counterparts due to the synergistic effect and the electronic effect [16]. Among all these bimetal nanoparticles, Au-Pt bimetallic nanoparticles with intrinsic peroxidase-like activity have been widely used in electrochemical immunoassay [17]. The nanoscale gold reduces binding energy between Pt and O through increasing the orbital overlap between neighboring atoms, down-shifting the d-band center, by which oxygen reduction reaction kinetic is enhanced [16].

Au@Pt core/shell nanoparticles are among the most common types of bimetallic nanoparticles. They have been widely applied in electrochemical immunoassays for their good biocompatibility and excellent catalytic capabilities for the reduction of hydrogen peroxide (H_2O_2) [18]. Lei and his colleagues presented a sensitive electrochemical immunoassay for the detection of alpha fetoprotein (AFP) by using graphene loaded bimetallic Au@Pt nanodendrites as signal tag [19]. Li's group developed a ultrasensitive electrochemical immunoassays for quantitative detection of squamous cell carcinoma antigen (SCCA) by using $Co_3O_4@CeO_2$-Au@Pt nanocomposite as enzyme-mimetic labels [20]. However, on one hand, due to its limited nature reserve and high cost, the usage of Pt in electrochemical immunoassay has to be reduced before this technology can be commercialized. On the other hand, there is a reciprocal relationship between the Pt shell thicknesses of Au@Pt core/shell nanoparticle and catalytic activity [21]. If the thickness of Pt shell is appropriate, the catalytic activity will reach a higher level. When it is applied in electrochemical immunoassay, high catalytic activity will increase the sensitivity of the method. Therefore, in order to improve utilization efficiency of the Pt and increase the sensitivity of the electrochemical immunoassay, tailored core/shell nanoparticles with an ideal Pt shell thickness is necessary. In addition, the thickness of the Pt shell on the surface of Au@Pt core/shell nanoparticles can be easily controlled via changing the molar ratio of H_2PtCl_6 to $HAuCl_4$ [22]. And to the best of our knowledge, there is no report focusing on optimizing the thickness of Pt shell when Au@Pt core/shell nanoparticles acted as label in electrochemical immunoassay.

In this work, we describe a novel sandwich-type electrochemical immunoassay for *E.coli* O157: H7 by using highly active electrocatalyst Au@Pt core/shell nanoparticles functionalized graphene nanocomposites and MNPs. On one hand, $Fe_3O_4@SiO_2$ were modified with primary antibody (Ab_1) acted as capture probe (denoted as $Fe_3O_4@SiO_2$-Ab_1). On the other hand, the Au@Pt core/shell nanoparticles achieved the highest catalytic effect through changing the molar ratios of Au to Pt. And the neutral red (NR) functionalized rGO (rGO-NR) possessed high surface area and strong chemical stability. It provided the ideal support for the homogeneous dispersion of Au@Pt nanoparticles (denote as rGO-NR-Au@Pt). The rGO-NR-Au@Pt nanocomposite were used to connect the secondary antibody (Ab_2) and horseradish peroxides (HRP) by the stable Au-N and Pt-N bond (denoted as rGO-NR-Au@Pt-Ab_2-HRP) [23]. Here, HRP not only served as an electrocatalytic reagent to increase the sensitivity of the method, but also blocked nonspecific sites as bovine serum albumin (BSA) did [24]. Once the *E.coli* O157: H7 existed, the "sandwich structure" was formed by the specific interactions between antigen and antibody. The sandwich immunocomplexes (denoted as $Fe_3O_4@SiO_2$-Ab_1/*E. coli* O157:H7/rGO-NR-Au@Pt-Ab_2-HRP) were attached on the surface of the working electrodes of 4 channel screen printed carbon electrode (4-SPCE) by an external magnet. Here, 4-SPCE was used to shorten the detection time and improve the reproducibility. Cyclic Voltammetry (CV) was employed to quantify *E. coli* O157:H7 via changes of the reduction peak current in the substrate solution of H_2O_2 with the thionine as electron mediator. Details of the preparation, characterization and possible application of the immunoassay are discussed as follows.

Experimental

Preparation of Au@Pt core/shell nanoparticles with different Pt shell thickness

The reagents, apparatus are provided in Electronic Supplementary Material. The Au@Pt core/shell nanoparticles were prepared according to the reference [22, 25]. In a typical synthesis of core/shell nanoparticles (Pt/Au molar ratio = 2.0), 1 wt% $HAuCl_4$ (0.5 mL) was added to 50 mL of double distilled water and the solution was heated to boil with stirring. Then 1 wt% sodium citrate (0.5 mL) was quickly introduced to the above solution. After heating for 15 min, the deep red solution appeared, indicating the formation of gold

nanoparticles. Then, 1.0 mL of 0.1 M ascorbic acid (excess) was subsequently added to the above deep red boiling solution, followed by adding 1.25 mL of 1 wt% H_2PtCl_6. After 20 min of heating, the black solution were obtained, which demonstrated that the Au@Pt core/shell nanoparticles were generated (See Scheme 1a).

For the preparation of the Au@Pt core/shell nanoparticles with different Pt shell thicknesses, Pt/Au molar ratios in the starting solution were varied from 0.0 to 4.0 (0:1, 1:2, 1:1, 2:1, 3:1, 4:1). The added amount of $HAuCl_4$ was fixed to 0.5 mL, while the added amount of H_2PtCl_6 was changed from 0.0 mL to 2.5 mL (0 mL, 0.3125 mL, 0.625 mL, 1.25 mL, 1.875 mL, and 2.5 mL). And all the other experiment conditions remained the same.

Preparation of rGO-NR-Au@Pt-Ab_2-HRP

The preparation of GO, rGO-NR and rGO-NR-Au@Pt are shown in Electronic Supplementary Material. 2 mL rGO-NR-Au@Pt dispersion was mixed with 2 mL PB, then 100 μL Ab_2 (80 μg·mL^{-1}) was added dropwise into it and oscillated at 4 °C for 3 h. Next, 500 μL HRP with a concentration of 5 mg·mL^{-1} was injected into the dispersion above and kept it for 2 h. Then, the solution was put in the refrigerator for 12 h. Finally, the dispersion was centrifuged and rinsed with PBS (pH = 7.4) to remove the unbound Ab_2 and HRP. Finally, the sediment was re-dispersed in 1 mL of PBS (pH = 7.4) and stored at 4 °C for future use (See Scheme 1b and c).

Preparation of Fe_3O_4@SiO_2-Ab_1

The synthesis of MNPs and Fe_3O_4@SiO_2 magnetic nanoparticles are provided in Electronic Supplementary Material. 250 μL Fe_3O_4@SiO_2 were ultrasonically resuspended in the mixed solution of 10 mL ethanol and 40 μL 3-aminopropyltriethoxysilane (APTES). And then the mixed solution was stirred overnight at room temperature so as to complete the silanized reaction. After reaction, the mixture was isolated by a magnet and washed several times with ethanol and PBS, respectively. Then, the amino-modified silica-coated Fe_3O_4 (Fe_3O_4@SiO_2-NH_2) was used to conjugate the antibody.

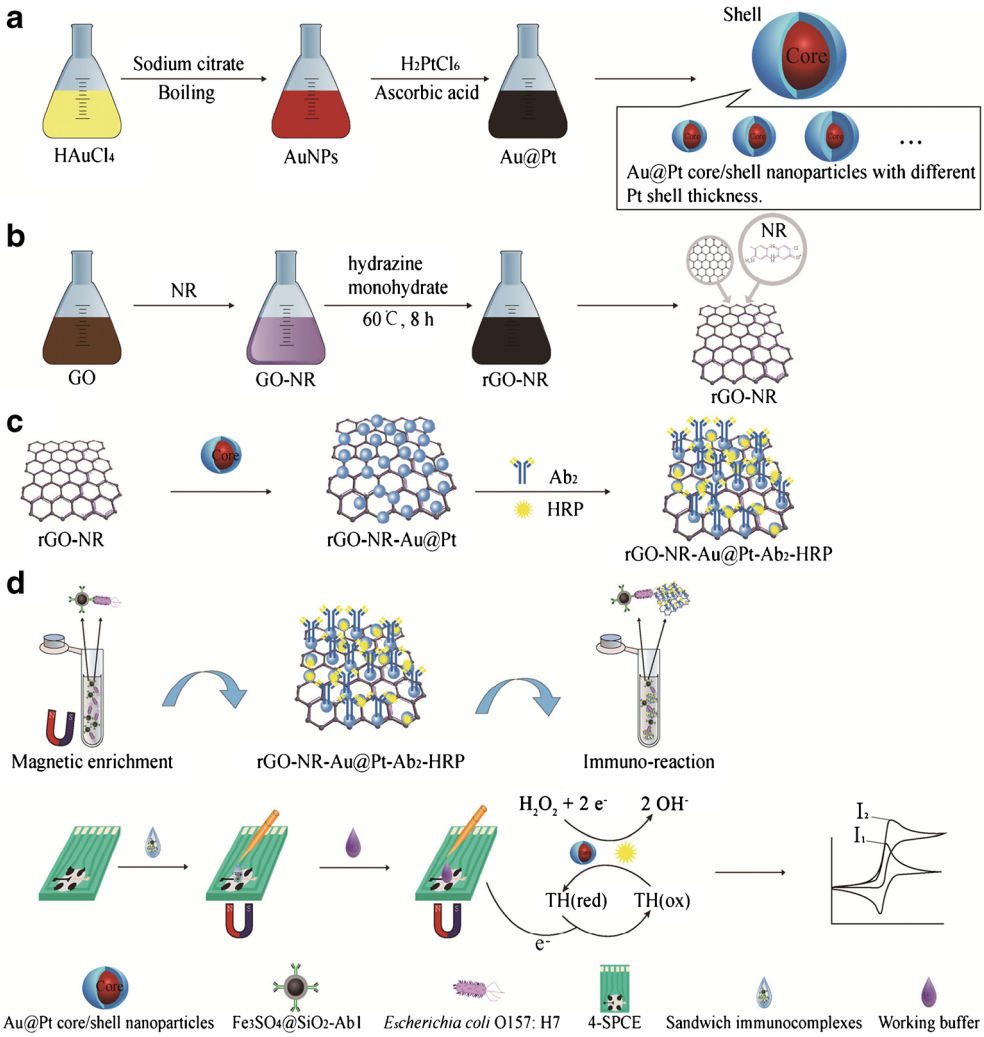

Scheme 1 Preparation of Au@Pt core/shell nanoparticles with different Pt shell thickness (**a**), rGO-NR (**b**), rGO-NR-Au@Pt-Ab_2-HRP (**c**) and the preparation and the detection process of the immunoassays (**d**)

N-(3-Dimethylaminopropyl)-N′-ethylcarbodiimide hydrochloride (EDC) and N-Hydroxysuccinimide (NHS) were used to activate the carboxyl of the antibody [26]. Briefly, 48.0 mg EDC and 60.0 mg NHS was dispersed in 1.2 mL PBS (pH 7.4), which was put in a centrifuge tube. Then 100 μL Ab_1 (145 $\mu g \cdot mL^{-1}$) was added into the solution. After incubation at 4 °C overnight, 200 μL $Fe_3O_4@SiO_2$-NH_2 was dispersed into the centrifuge tube. In order to improve the efficiency of the reaction, the centrifuge tube was placed in a shaking table for 4 h at room temperature. Finally, $Fe_3O_4@SiO_2$-Ab_1 was collected with the help of a magnet and washed three times with PBS (pH 7.4). The prepared resultant $Fe_3O_4@SiO_2$-Ab_1 were dispersed in 200 μL of PBS and stored at 4 °C for further use.

Fabrication of the immunoassay

The preparation of bacterial antigen are shown in Electronic Supplementary Material. 1.0 mL of *E. coli* O157:H7 sample with different concentration was dropped in a centrifuge tube. Subsequently, 25 μL $Fe_3O_4@SiO_2$-Ab_1 were added into the tube. The mixture was incubated for 60 min at 37 °C and washing three times with a magnet to remove redundant *E. coli* O157:H7. Next, 125 μL rGO-NR-Au@Pt-Ab_2-HRP were added into the above isolates in the centrifuge tube and incubated for another 60 min at 37 °C. After specific recognition of antigen and antibody, the "sandwich structure" was formed (denote as $Fe_3O_4@SiO_2$-Ab_1/*E. coli* O157:H7/rGO-NR-Au@Pt-Ab_2-HRP). The sandwich immunocomplexes were separated by a magnet and washed by PBS (pH 7.4) for three times. Finally, the sandwich immunocomplexes were re-dispersed in 25 μL PBS and stored at 4 °C for further use.

Electrochemical determination of *E. coli* O157:H7

Scheme 1d displays the preparation process of the immunoassay. Each working electrode of the 4-SPCE (the choice of 4-SPCE is discussed in Electronic Supplementary Material) were absorbed 3 μL of sandwich immunocomplexes by a magnet. 300 μL HAC-NaAc (pH = 5.5, 0.1 $mol \cdot L^{-1}$) containing 1.0 $mmol \cdot L^{-1}$ TH and 5.0 $mmol \cdot L^{-1}$ H_2O_2 (working buffer) was dropped on the above modified electrode. The detection of *E. coli* O157:H7 was performed by measuring the reduction peak current change (ΔI_{pc}) of cyclic voltammetry (CV) before and after the sandwich immunocomplexes were put on the electrode. Before the sandwich immunocomplexes were absorbed on the electrode, the reduction peak current response was recorded as I_1. After the sandwich immunocomplexes were absorbed on the electrode by the magnet, the Au@Pt core/shell nanoparticles and HRP in rGO-NR-Au@Pt-Ab_2-HRP catalyzed H_2O_2 in working buffer to hydroxyl ions. Thus, the increased reduction peak current response was recorded as I_2. Therefore, ΔI_{pc} was expressed as $\Delta I_{pc} = I_2 - I_1$. Considering the convenient operation and practical application of the immunoassay, the electrochemical experiments were carried out at room temperature. All experimental solutions were deaerated by nitrogen for at least 15 min. During the detection process, the potential was swept from −0.6 to 0.1 V (vs. Ag/AgCl) with a CHI 1030 at scan rate of 50 $mV \cdot s^{-1}$. Three successive CV scans were performed for each measurement, and the last cycle was recorded.

Results and discussion

Characterization of Au@Pt core/shell nanoparticles with different Pt shell thickness

Au@Pt core/shell nanoparticles with different Pt shell thickness were prepared through changing the molar ratios of H_2PtCl_6 to $HAuCl_4$ in starting precursor solution. In order to demonstrate they have been prepared successfully, we choose high-resolution transmission electron microscopy (HRTEM) to characterize the Au@Pt core/shell nanoparticles synthesized with different Pt/Au molar ratio (1:1, 2:1, 4:1). Figure 1a, b, c are the HRTEM micrographs of the solution with the Pt/Au molar ratio of 1:1, 2:1, 4:1, respectively. Fig. 1d, e and f are the corresponding TEM micrographs with low magnification. As can be seen from HRTEM, the structure of nanoparticles is core/shell shape. According to the reduction sequence, the core is the Au and the shell Pt [21]. From the TEM micrographs with low magnification, no other isolated Pt or Au nanostructures are observed, which also indicate that the formation of core/shell structure. Figure 1d, e and f show that the Pt shell thickness (or density) and the size of nanoparticles are increased with the increase of Pt/Au molar ratio. Therefore, we draw the conclusion that Pt shell thickness of Au@Pt core/shell nanoparticles is controllable through changing the molar ratios of H_2PtCl_6 to $HAuCl_4$ in starting precursor solution.

The growth of the Pt shell on gold nanoparticles (AuNPs) surface can be readily monitored by UV-visible spectroscopy. Figure 2a shows the UV-vis spectra of Au@Pt core/shell nanoparticles from various solutions with different Pt/Au molar ratio. The Au nanoparticles without a Pt shell clearly shows an absorption peak centered at 520 nm (curve a), which is due to the surface plasmon resonance (SPR) of AuNPs. Upon Pt shell growth, the SPR of the Au@Pt core/shell nanoparticles show wide adsorption in the visible region. It is noted that the high Pt/Au molar ratio exhibits a wider visible absorption peak than that of low Pt/Au molar ratio. And for higher Pt/Au molar ratio, the absorption peak gradually diminishes and suppresses. This may be attributed to the following fact. With the increase of Pt/Au molar ratio, the Pt shell thickness is increased [27, 28]. However, Pt shell has no characteristic absorption in the visible-near-infrared spectroscopy [22],

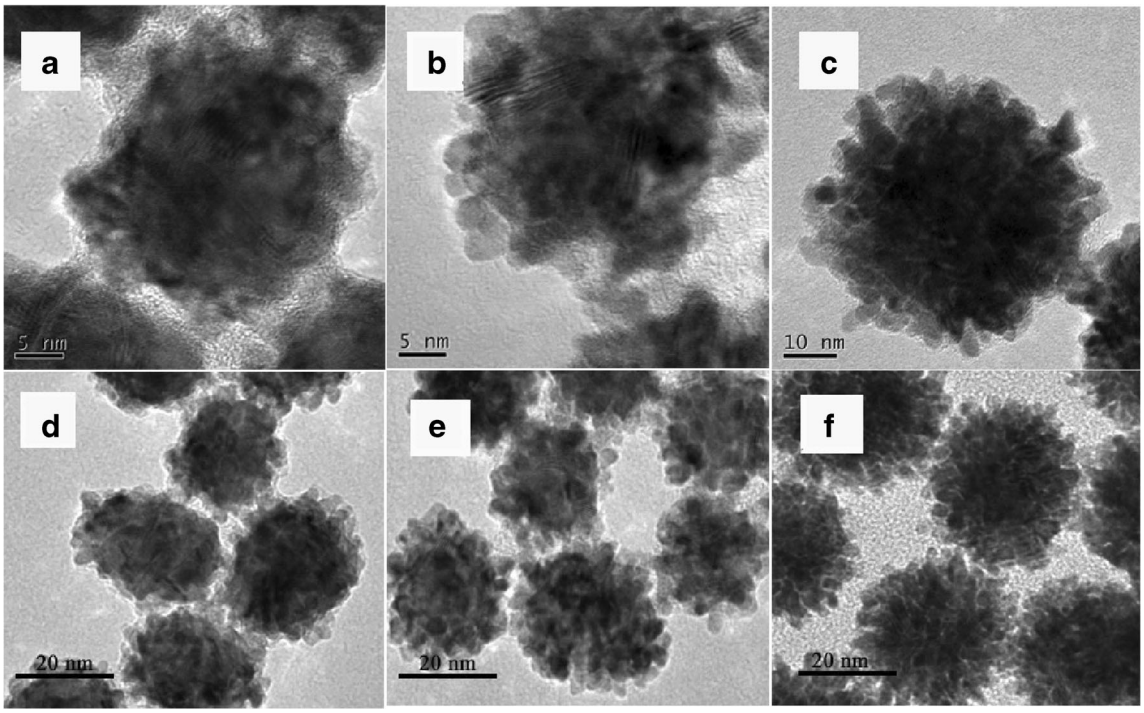

Fig. 1 HRTEM images of Au@Pt core/shell nanoparticles with Pt/Au molar ratio of (**a**) 1:1, (**b**) 2:1, (**c**) 4:1. Low-magnification TEM of Au@Pt core/shell nanoparticles with Pt/Au molar ratio of (**d**) 1:1, (**e**) 2:1, (**f**) 4:1

which results that the Au plasmon absorption peak become suppressed with the increase of surface coverage of Pt shell. The suppression with the increase of Pt/Au molar ratio also indicates a continuous increase in the shell thickness. The scattering by the Pt shell and the change in the dielectric that surrounds the gold may be an important factor [22]. Figure 2b is the digital photographs of Au@Pt core/shell nanoparticles with different Pt shell thickness. With the increase of Pt/Au molar ratio, the color of the solution gradually changes from wine-red to dark black. This result is caused by growth of the

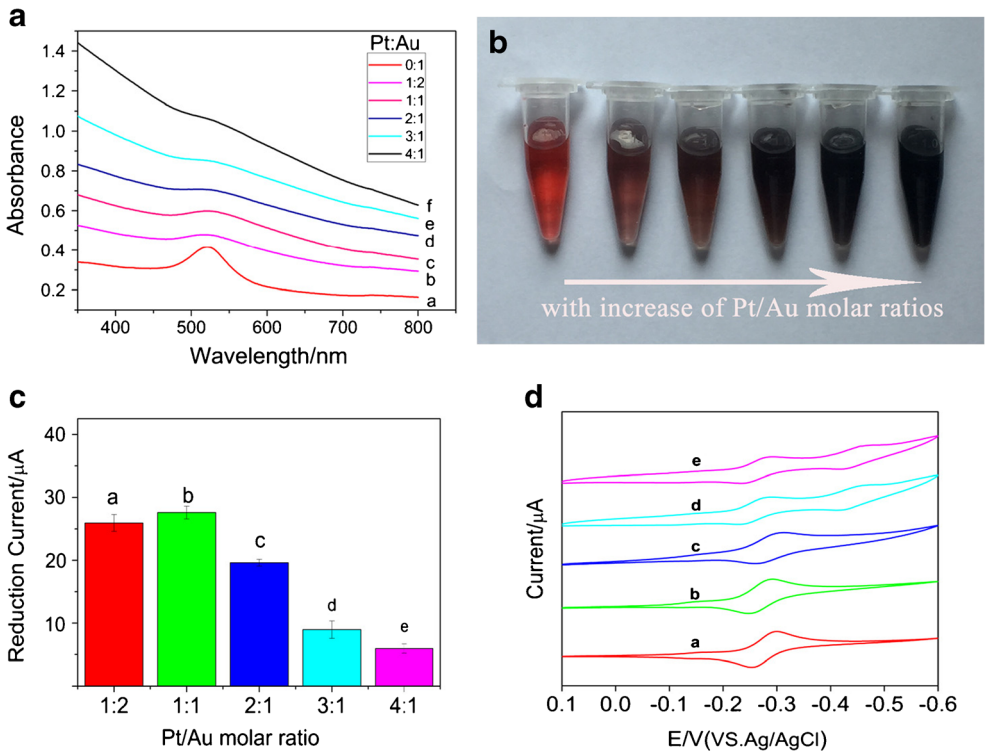

Fig. 2 **a** UV-vis spectra of (*a*) AuNPs and (*b-f*) Au@Pt core/shell nanoparticles with different Pt/Au molar ratio. **b** Digital photographs of Au@Pt core/shell nanoparticles taken at different Pt/Au molar ratios. c Reduction peak current of Au@Pt core/shell nanoparticles with different Pt/Au molar ratio and (**d**) corresponding CV curves in HAC-NaAc (pH = 5.5, 0.1 mol·L^{-1}) containing 5.0 mmol·L^{-1} H_2O_2 with 1.0 mmol·L^{-1} TH

Pt shells on the Au cores. If the proportion of Pt is higher, the color of the solution is darker. This finding is in accordance with the result for UV-visible spectroscopy measurements. In a word, we have successfully prepared Au@Pt core/shell nanoparticles with different Pt shell thickness by changing Pt/Au molar ratio.

Choice of highly active electrocatalyst Au@Pt core/shell nanoparticles

The catalytic activity of Au@Pt core/shell nanoparticles is relevant to the Pt shell thicknesses [21]. In order to increase the sensitivity of the immunoassay, the highest catalytic active Au@Pt core/shell nanoparticles are chosen to develop the electrochemical immunoassay. The 4-SPCE was coated by Au@Pt core/shell nanoparticles (3 μL) with different Pt/Au molar ratio (1:2, 1:1, 2:1, 3:1 and 4:1) respectively and dried at room temperature. The Au@Pt core/shell nanoparticles have electrocatalytic activity for the reduction of H_2O_2, the detection solution was HAC-NaAc (pH = 5.5, 0.1 mol·L^{-1}) containing 5.0 mmol·L^{-1} H_2O_2 with 1.0 mmol·L^{-1} TH as mediators. Figure 2c is the reduction peak current of working electrode modified by Au@Pt core/shell nanoparticles with different Pt/Au molar ratio, and Fig. 2d is the corresponding CV curves. It shows that the reduction peak current is highest when the Pt/Au molar ratio is 1:1 and slightly higher than the ratio of 1:2. With the further increase of Pt/Au molar ratio, the catalytic activity of Au@Pt core/shell nanoparticles is dramatically decreased. In this work, when Pt/Au molar ratio is 1:1, Au@Pt core/shell nanoparticles possess the highest catalytic ability and the utilization efficiency of the Pt is highest. The electrocatalytic reaction is depend on the accessibility of the reactants to the catalysts [29]. That is to say, the value of reduction peak current is depending on the accessibility of the H_2O_2 to the Pt. The Au@Pt core/shell nanoparticles with higher Pt/Au molar ratio have a thicker Pt shell, which results that H_2O_2 can't gain access to inner parts of the Pt shell. But a thinner Pt shell may be not enough to catalyze excess H_2O_2. Therefore, we choose Au@Pt core/shell nanoparticles with the Pt/Au molar ratio of 1:1 in the latter experiment.

Agglutination test

Agglutination test is used to verify the anti-*E. coli* O157:H7 (Ab_1 and Ab_2) had successfully linked with Fe_3O_4@SiO_2-NH_2 and rGO-NR-Au@Pt (The Characterization of rGO-NR, rGO-NR-Au@Pt, MNPs, Fe_3O_4@SiO_2, and Fe_3O_4@SiO_2-NH_2 nanoparticles are provided in Electronic Supplementary Material). 10 μL *E. coli* O157:H7 (10^9 CFU·mL^{-1}) was dropped on glass slide, then 10 μL Fe_3O_4@SiO_2-Ab_1 suspension and 10 μL rGO-NR-Au@Pt-Ab_2-HRP suspension were mixed with *E. coli* O157:H7, respectively. The result was recorded after reacting for 1 min. *C. sakazaki*, *E. coli* ATCC 8739, *C. freundii* and PBS were used as control groups. As can be seen from Fig. S3A, Fe_3O_4@SiO_2-Ab_1 are uniformly dispersed in other four groups, but appearing agglutination blocks in *E. coli* O157:H7 group. Similarly, the result is the same in rGO-NR-Au@Pt-Ab_2-HRP (see Fig. S3B). This confirms that anti-*E. coli* O157:H7 (Ab_1 and Ab_2) have been successfully linked with Fe_3O_4@SiO_2-NH_2 and rGO-NR-Au@Pt, respectively. These two nanocomposites possess good specificity to *E. coli* O157:H7.

Cyclic voltammetry

CV measurement was used to characterize the effect of each component on the electrode after each modified step. Each step was recorded in HAC-NaAc (pH = 5.5, 0.1 mol·L^{-1}) containing 1.0 mmol·L^{-1} TH and 5.0 mmol·L^{-1} H_2O_2. Figure 3*a* shows a pair of reversible redox peaks of TH at bare 4-SPCE. After Fe_3O_4@SiO_2-Ab_1 are dropped on the 4-SPCE, the redox current slightly decreases (curve b). This is mainly ascribed to the non-conductive SiO_2 and Ab_1. The redox current continues decreasing after Fe_3O_4@SiO_2-Ab_1 combine with *E. coli* O157:H7 (curve c). This result indicates that Fe_3O_4@SiO_2-Ab_1 and *E. coli* O157:H7 have been combined together through the specific binding affinity between antigen and antibody. After rGO-NR-Au@Pt-Ab_2-HRP are incubated with Fe_3O_4@SiO_2-Ab_1/*E. coli* O157:H7 (curve d), an obvious increase of the reduction current and a decrease of the oxidation current are observed. This suggests that the "sandwich structure" is formed. The catalytic current mainly derived from the highly catalytic activity of Au@Pt core/shell nanoparticles and HRP toward the reduction of H_2O_2.

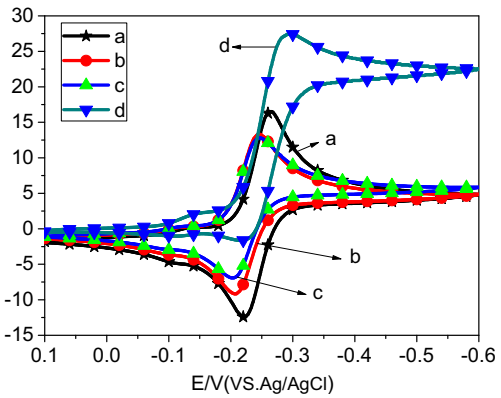

Fig. 3 CVs of different modified electrodes in HAC-NaAc (pH = 5.5, 0.1 mol·L^{-1}) containing 1.0 mmol·L^{-1} TH and 5.0 mmol·L^{-1} H_2O_2: (*a*) bare 4-SPCE (Star), (*b*) 4-SPCE/Fe_3O_4@SiO_2-Ab_1 (Circle), (*c*) 4-SPCE/Fe_3O_4@SiO_2-Ab_1/*E. coli* O157:H7 (Up Triangle), (*d*) 4-SPCE/Fe_3O_4@SiO_2-Ab_1/*E. coli* O157:H7/ rGO-NR-Au@Pt-Ab_2-HRP (Down Triangle)

Comparison of electrochemical responses using various signal tags

To clarify the advantage of the immunoassay using rGO-NR-Au@Pt-Ab_2-HRP immunocomplex as signal amplification section, a comparative study of the electrochemical responses of the immunoassays was carried. The immunoassays are built with four types of signal probes, including Au@Pt-Ab_2 (Pt/Au molar ratio = 1) (Fig. 4a), rGO-NR-Au@Pt-Ab_2 (Pt/Au molar ratio = 2) (Fig. 4b), rGO-NR-Au@Pt-Ab_2 (Pt/Au molar ratio = 1) (Fig. 4c), rGO-NR-Au@Pt-Ab_2-HRP (Pt/Au molar ratio = 1) (Fig. 4d). During the measurement process, the same capture probe Fe_3O_4@SiO_2-Ab_1 was used to incubate with *E. coli* O157:H7 (4.0×10^7 CFU·mL^{-1}). The sandwich immunocomplexes were detected in the absence (curve a, black line) and presence (curve b, red line) of H_2O_2. As shown in Fig. 4, the use of rGO-NR-Au@Pt-Ab_2 bioconjugate (Fig. 4b and c) offers greater current increase than that obtained with Au@Pt-Ab_2 bioconjugate (Fig. 4a). This is mainly attributed to the high surface-to-volume ratio of rGO, which increases the number of Au@Pt core/shell nanoparticles loaded and leads more Au@Pt to catalyze the reduction of H_2O_2. Compared Fig. 4b with Fig. 4c, the current increase of Fig. 4c is higher than that of Fig. 4b. This further confirms that the use of Au@Pt core/shell nanoparticles with the Pt/Au molar ratio of 1:1 can extremely amplify the electrochemical signal and play an important role in increasing the sensitivity of the immunoassay. And it can be found that the use of rGO-NR-Au@Pt-Ab_2-HRP (Pt/Au molar ratio = 1) bioconjugate offers the highest current increase (Fig. 4d) in all four signal tags. This suggests that HRP as electrocatalytic reagent can not only promotes signal amplification but also blocked nonspecific sites as BSA did. Therefore, rGO-NR-Au@Pt-Ab_2-HRP (Pt/Au molar ratio = 1) bioconjugate was chosen as tracer for the immunoassay to obtain superior signal amplification and increase the sensitivity of following experiments.

Electrochemical determination of *E. coli* O157:H7

In order to achieve better experimental results, the experimental conditions were optimized. The optimization of the experimental conditions is discussed in detail in Electronic Supplementary Material (Fig. S4). Under the optimal conditions, the immunoassay was used to detect a series of *E. coli* O157:H7 solutions. Figure 5a is the CV curve of each concentration of *E. coli* O157:H7. As indicated from Fig. 5b, the ΔI_{pc} of the electrochemical immunoassay increases with the increase of *E. coli* O157:H7 concentrations. It exhibits a linear

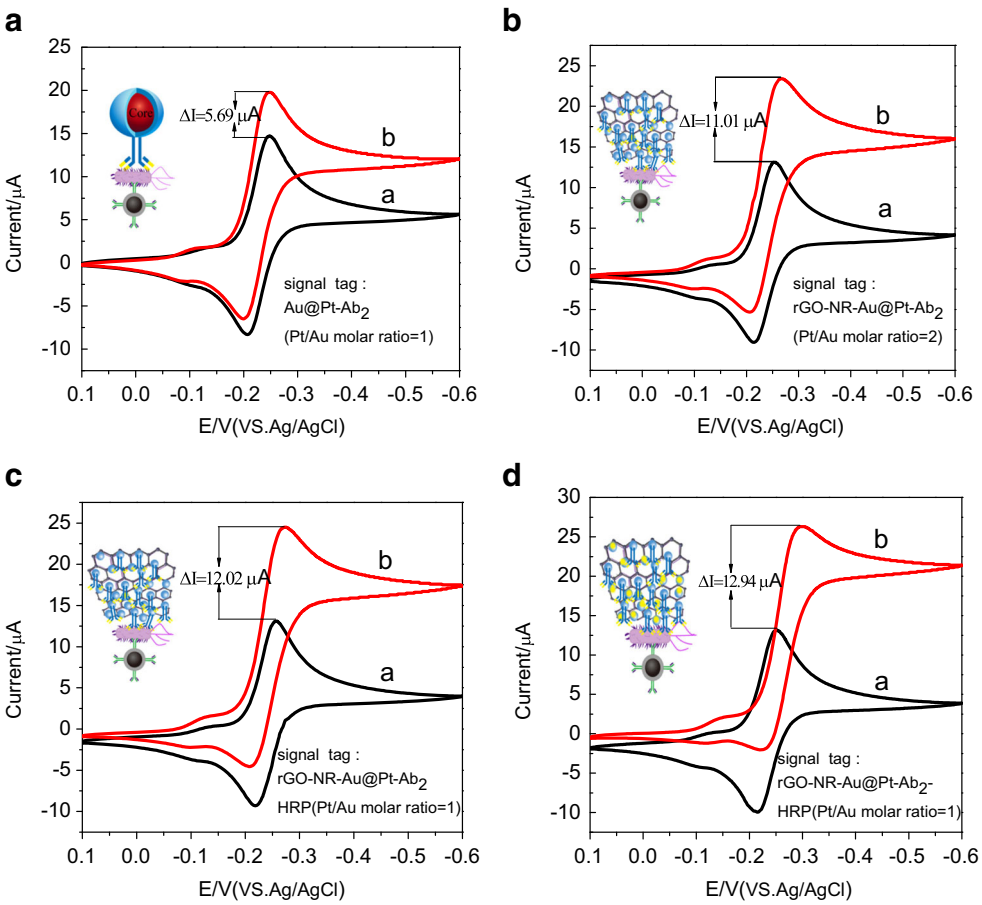

Fig. 4 CVs of different sandwich format immunoassays in the absence (curve a, black line) and presence of 5.0 mmol·L^{-1} H_2O_2 (curve b, red line) in HAC-NaAc (pH = 5.5, 0.1 mol·L^{-1}) containing 1.0 mmol·L^{-1} TH by using various signal tags: (**a**) Au@Pt-Ab_2 (Pt/Au molar ratio = 1), (**b**) rGO-NR-Au@Pt-Ab_2 (Pt/Au molar ratio = 2), (**c**) rGO-NR-Au@Pt-Ab_2 (Pt/Au molar ratio = 1), (**d**) rGO-NR-Au@Pt-Ab_2-HRP (Pt/Au molar ratio = 1)

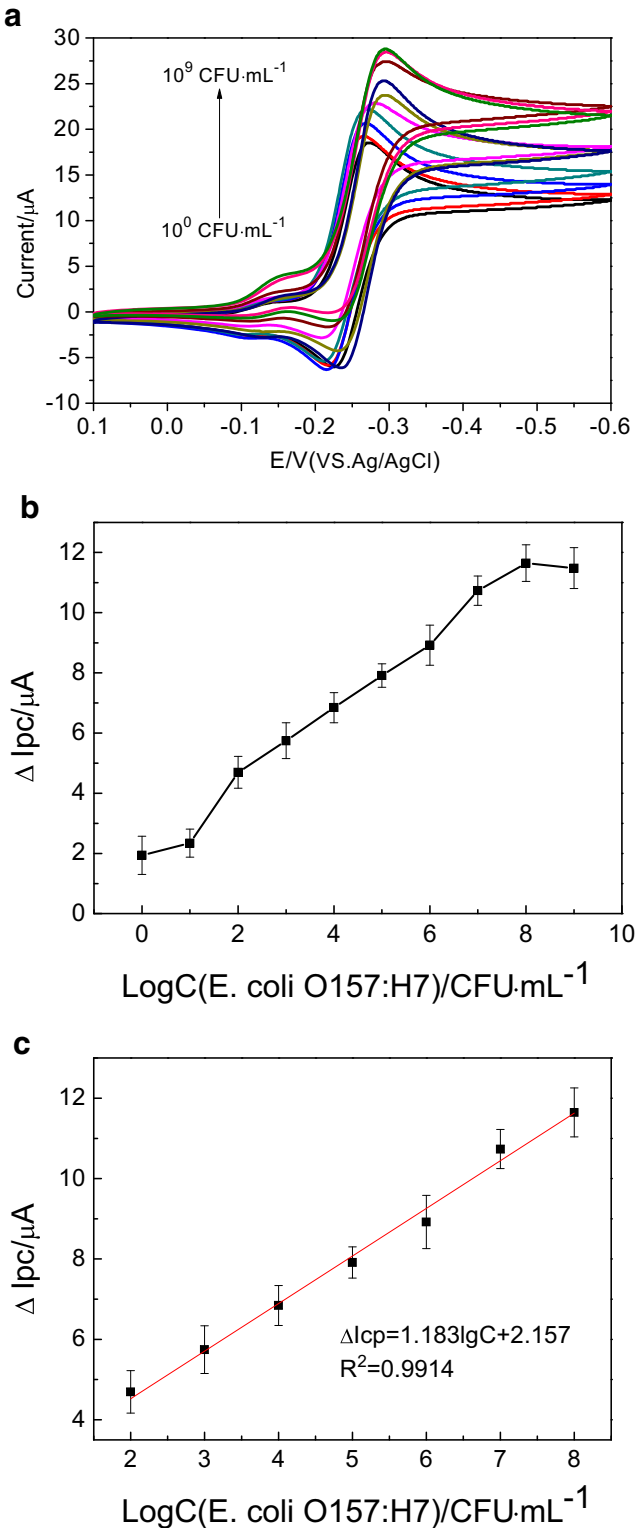

Fig. 5 **a** The CVs curve of different concentrations of *E. coli* O157:H7. **b** The ΔI_{pc} of different logarithmic concentrations of *E. coli* O157:H7. **c** Linear relation between the reduction peak current change (ΔI_{pc}) and the logarithmic of *E. coli* O157:H7 concentration

relationship between the ΔI_{pc} and the logarithm of the *E. coli* O157:H7 concentration in the range from 4.0×10^2 to 4.0×10^8 CFU·mL^{-1} (Fig. 5c). The regression equation of the calibration curve can be expressed as ΔI_{pc} (μA) = 1.183lgC + 2.157 with correlation coefficient of 0.9914 and limit of detection (LOD) of 9.1×10^1 CFU·mL^{-1} ($S/N = 3$). Compared with the previous reports for the detection of *E. coli* O157:H7 (as shown in Table 1), this method exhibits a relatively lower detection limit and a wider linear range. This enhanced performance is manily due to a great number of Au@Pt core/shell nanoparticles with highly catalytic activity are loaded on the large specific surface of rGO. Besides, the HRP can catalyze the oxidation reaction of TH by H_2O_2. And Fe_3O_4@SiO_2-Ab_1 acted as capture probe can increase the sensitivity of the method by magnetic enrichment.

Specificity, reproducibility and stability of the immunoassay

The specificity of the immunoassay is evaluated by challenging the system against other bacteria including *C. sakazakii*, *C. freundii* and *E. coli* ATCC 8739. In addition, all of the bacteria solution concentrations were 10^7 CFU·mL^{-1}, PBS was used as a blank control. It can be seen from Fig. 6, only *E. coli* O157:H7 leads to an obvious ΔI_{pc}. Additionally, we used the immunoassay for *E. coli* O157:H7 analysis in the coexistence of other bacteria. As shown in Fig. 6, the coexistence of other tested bacteria almost have no effect on the current response of the immunoassay to *E. coli* O157:H7. The results demonstrate that this immunoassay is highly selective for *E. coli* O157:H7 detection.

In order to evaluate the reproducibility of this electrochemical immunoassay, a series of five different electrodes are used to detect *E. coli* O157:H7 (4.0×10^7 CFU·mL^{-1}) (Fig. S5A).The relative standard deviation (RSD) of the measurements for these five working electrodes is less than 5%, indicating good reproducibility.

The stability plays an important role in the application of the immunoassay. The prepared Fe_3O_4@SiO_2-Ab_1 and rGO-NR-Au@Pt-Ab_2-HRP are stored at 4 °C, and the detection result is depicted in Fig. S5B. After storage for 1, 2, 3, 4 and 5 weeks, there is no apparent ΔI_{pc} variation of the immunoassay for detection of the same concentration of *E. coli* O157:H7. The results indicate the acceptable stability of the immunoassay.

Real sample analysis

In order to further prove the reliability of the immunoassay, the recovery of *E. coli* O157:H7 in spiked pork and milk

Table 1 Comparison of different methods for the determination of *E. coli* O157:H7

Methods	Signal strategies	Linearity range (CFU·mL^{-1})	LOD (CFU·mL^{-1})	Ref.
EIS	Label-free	$1.0 \times 10^{2-}1.0 \times 10^{7}$	100	[30]
Electroanalysis	Ag@SiO_2	$20–8.0 \times 10^{3}$	13	[31]
Electroanalysis	Label-free	$4.12 \times 10^{2}–4.12\times 10^{5}$	250	[32]
Fluorescent	BODDIP and BHQ2	$2.0 \times 10^{2}–1.0 \times 10^{7}$	200	[33]
CL	Glucose oxidase and laccase	$4.3 \times 10^{3}–4.3 \times 10^{5}$	<1200	[34]
Colorimetric	E17F-37 and E18R-42	$1.0 \times 10^{4}–1.0 \times 10^{8}$	104	[35]
Lateral flow immunoassays	Gold-decorated polystyrene particles	–	100	[36]
Magnetoimpedance	Dynabeads	$5.0 \times 10^{1}–5.0 \times 10^{2}$	50	[37]
Electroanalysis	rGO-NR-Au@Pt-Ab2-HRP	$4.0 \times 10^{2}–4.0 \times 10^{8}$	91	This work

LOD limit of detection, *EIS* Electrochemical impedance spectroscopy, *CL* Chemiluminescence

samples were detected by standard addition method. The pork samples were homogenized by a pat type sterile homogenizer and the milk samples were diluted by PBS. The pork and milk samples were spiked *E. coli* O157:H7 with a final concentration of 4.0×10^{2}, 4.0×10^{5} and 4.0×10^{8} CFU·mL^{-1}, which were certified by flat counting method. Through the samples analysis, the recovery is within the range of 89.0–107.5% in the pork and 95.0–105.8% in the milk (Table 2). In order to better verify the application of this immunoassay in practical sample detection,the immunoassay was compared with the standard culture method for the detection of *E. coli* O157:H7 through the accuracy. Based on the specific experimental results of this immunoassay, if ΔI_{pc} of the test sample is less than 3.0 μA, the sample is negative; otherwise, the sample is positive. As shown in Table S1, the accuracy rate is 100 and 100% in pork and in milk samples, respectively. These two experiments suggest that the immunoassay hold great promise as a reliable tool for the detection of *E. coli* O157:H7 in real samples.

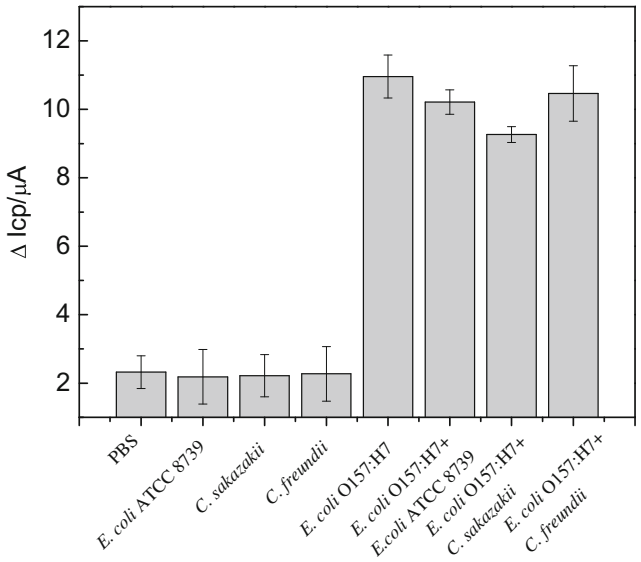

Fig. 6 Specificity of the immunoassay toward: PBS, *E. coli* ATCC 8739, *C. sakazakii*, *C. freundii* and *E. coli* O157:H7; and *E. coli* ATCC 8739, *C. sakazakii* and *C. freundii* were mixed with *E. coli* O157:H7, respectively

Conclusion

This work described highly sensitive electrochemical immunoassay for *E. coli* O157: H7 based on highly catalytic active Au@Pt core/shell nanoparticles functionalized rGO and Fe_3O_4 magnetic nanoparticles. The rGO-NR nanocomposites as immunoassay platform can provide a high density of Au@Pt core/shell nanoparticles because of their high surface area. Au@Pt core/shell nanoparticles here can act as desirable scaffold with large surface area for efficient immobilization of antibody and HRP. The method combined the nanocatalytic properties of the redox-active nanoparticles and the bioelectrocatalytic amplification of the bioactive enzyme and exhibited acceptable specificity, reproducibility and stability.

Table 2 Determination of *E. coli* O157:H7 in pork and milk samples

Sample	Spiked (CFU·mL^{-1})	Found (CFU·mL^{-1})	Recovery (%)	RSD (%, $N = 5$)
Pork1	4.0×10^{2}	3.56×10^{2}	89.0	4.0
Pork2	4.0×10^{5}	3.92×10^{5}	98.0	2.3
Pork3	4.0×10^{8}	4.30×10^{8}	107.5	2.1
Milk1	4.0×10^{2}	3.80×10^{2}	95.0	4.6
Milk2	4.0×10^{5}	3.98×10^{5}	99.5	3.0
Milk3	4.0×10^{8}	4.23×10^{8}	105.8	2.4

However, the electrochemical immunoassay needs to be improved when it is applied in real sample and the recovery in low concentration samples is relatively low. And the preparation of the nanomaterial is relatively complex. The research provides a guide to develop of rGO-NR-Au@Pt based immunoassay for sensitive and quantitative analysis other pathogenic bacteria. And the bio-sensing system can also be easily extended to other biomedical applications employing known specific binding of target and labels.

Acknowledgements This work was financially supported by a grant from National Natural Science Foundation of Zhejiang Province (LY17C200003), the Food and Engineering most important discipline of Zhejiang province (2017SIAR210, JYTSP20141062), Zhejiang public Innovation Platform Analysis and testing project (2018C37056) and plans of college students in Zhejiang province and technology innovation activities (acrobatic tender grass talent programme) project (2017R408053, 2017R408054), open fund of State Key Laboratory for Diagnosis and Treatment of Infectious Diseases, The First Affiliated Hospital of Medical College,Zhejiang University (2017KF02).

Compliance with ethical standards

The authors declare that we have no conflict of interest.

Ethical approval This article does not contain any studies with animals performed by any of the authors.

Informed consent Informed consent was obtained from all individual participants included in the study.

References

1. Lin H, Lu Q, Ge S, Cai Q, Grimes CA (2010) Detection of pathogen Escherichia coli O157:H7 with a wireless magnetoelastic-sensing device amplified by using chitosan-modified magnetic Fe 3 O 4 nanoparticles. Sensors Actuators B Chem 147(1):343–349
2. Hassan AR, De lEA, Merkoçi A (2015) Highly sensitive and rapid determination of Escherichia coli O157:H7 in minced beef and water using electrocatalytic gold nanoparticle tags. Biosens Bioelectron 67:511–515
3. Yang L, Bashir R (2008) Electrical/electrochemical impedance for rapid detection of foodborne pathogenic bacteria. Biotechnol Adv 26(2):135–150
4. De BE, Beumer RR (1999) Methodology for detection and typing of foodborne microorganisms. Int J Food Microbiol 50(1–2):119–130
5. Roda A, Mirasoli M, Roda B, Bonvicini F, Colliva C, Reschiglian P (2012) Recent developments in rapid multiplexed bioanalytical methods for foodborne pathogenic bacteria detection. Microchim Acta 178(1–2):7–28
6. Zhu T, Hu Y, Yang K, Dong N, Yu M, Jiang N (2018) A novel SERS nanoprobe based on the use of core-shell nanoparticles with embedded reporter molecule to detect E. coli O157:H7 with high sensitivity. Microchim Acta 185(1):30. https://doi.org/10.1007/s00604-017-2573-9
7. Guo Y, Wang Y, Liu S, Yu J, Wang H, Liu X, Huang J (2017) Simultaneous voltammetric determination of E. coli and S. Typhimurium based on target recycling amplification using self-assembled hairpin probes on a gold electrode. Microchim Acta 184(3):745–752. https://doi.org/10.1007/s00604-016-2017-y
8. Ye W, Chen T, Mao Y, Tian F, Sun P, Yang M (2017) The effect of pore size in an ultrasensitive DNA sandwich-hybridization assay for the Escherichia coli O157:H7 gene based on the use of a nanoporous alumina membrane. Microchim Acta 184(12):4835–4844. https://doi.org/10.1007/s00604-017-2530-7
9. Gan C, Wang B, Huang J, Qileng A, He Z, Lei H, Liu W, Liu Y (2017) Multiple amplified enzyme-free electrochemical Immunosensor based on G-Quadruplex/hemin functionalized mesoporous silica with redox-active intercalators for microcystin-LR detection. Biosens Bioelectron 98:126–133
10. Wang R, Feng JJ, Liu WD, Jiang LY, Wang AJ (2017) A novel label-free electrochemical immunosensor based on the enhanced catalytic currents of oxygen reduction by AuAg hollow nanocrystals for detecting carbohydrate antigen 199. Biosens Bioelectron 96:152–158
11. Fei J, Dou W, Zhao G (2015) A sandwich electrochemical immunosensor for Salmonella pullorum and Salmonella gallinarum based on a screen-printed carbon electrode modified with an ionic liquid and electrodeposited gold nanoparticles. Microchim Acta 182(13–14):2267–2275
12. Zhu C, Yang G, Li H, Du D, Lin Y (2015) Electrochemical sensors and biosensors based on nanomaterials and nanostructures. Anal Chem 87(1):230–249
13. Wang DW, Li F, Wu ZS, Ren W, Cheng HM (2009) Electrochemical interfacial capacitance in multilayer graphene sheets: dependence on number of stacking layers. Electrochem Commun 11(9):1729–1732
14. Hu N, Wang Y, Chai J, Gao R, Yang Z, Kong SW, Zhang Y (2012) Gas sensor based on p-phenylenediamine reduced graphene oxide. Sensors Actuators B Chem 163(1):107–114
15. Sun Q, Zhao G, Dou W (2016) An optical and rapid sandwich immunoassay method for detection of Salmonella pullorum and Salmonella gallinarum based on immune blue silica nanoparticles and magnetic nanoparticles. Sensors Actuators B Chem 226:69–75
16. Tang J, Tang D (2015) Non-enzymatic electrochemical immunoassay using noble metal nanoparticles: a review. Microchim Acta 182(13–14):2077–2089
17. Fan Y, Yang Z, Ying Z, Chai Y, Yuan R (2015) Ultrasensitive electrochemical immunosensor for carbohydrate antigen 19-9 using Au/porous graphene nanocomposites as platform and Au@Pd core/shell bimetallic functionalized graphene nanocomposites as signal enhancers. Biosens Bioelectron 66:356–362
18. Zhou J, Tang D, Li H, Cui Y, Chen H, Chen G (2012) Nanoplatinum-enclosed gold nanocores as catalytically promoted nanolabels for sensitive electrochemical immunoassay. Anal Chim Acta 751(21):52–58
19. Jiao L, Mu Z, Zhu C, Wei Q, Li H, Du D, Lin Y (2016) Graphene loaded bimetallic au@Pt nanodendrites enhancing ultrasensitive electrochemical immunoassay of AFP. Sensors Actuators B Chem 231:513–519
20. Li Y, Zhang Y, Li F, Feng J, Li M, Lei C, Dong Y (2017) Ultrasensitive electrochemical immunosensor for quantitative detection of SCCA using Co 3 O 4 @CeO 2 -Au@Pt nanocomposite as enzyme-mimetic labels. Biosens Bioelectron 92:33–39
21. Ataeeesfahani H, Wang L, Nemoto Y, Yamauchi Y (2010) Synthesis of bimetallic Au@Pt nanoparticles with Au core and nanostructured Pt Shell toward highly active Electrocatalysts. Chem Mater 22(23):6310–6318
22. Guo S, Wang L, Dong S, Wang E (2008) A novel Urchinlike gold/platinum hybrid Nanocatalyst with controlled size. J Phys Chem C 112(35):13510–13515
23. Roushani M, Valipour A (2015) Using electrochemical oxidation of Rutin in modeling a novel and sensitive immunosensor based on Pt nanoparticle and graphene–ionic liquid–chitosan nanocomposite to detect human chorionic gonadotropin. Sensors Actuators B Chem 222:1103–1111

24. Bai L, Yuan R, Chai Y, Yuan Y, Mao L, Wang Y (2011) Platinum-gold alloy nanoparticles and horseradish peroxidase functionalized nanocomposite as a trace label for ultrasensitive electrochemical detection of thrombin. Anal Chim Acta 698(1–2):14–19
25. Zan X, Fang Z, Wu J, Xiao F, Huo F, Duan H (2013) Freestanding graphene paper decorated with 2D-assembly of Au@Pt nanoparticles as flexible biosensors to monitor live cell secretion of nitric oxide. Biosens Bioelectron 49(35):71–78
26. Ma W, Chen W, Qiao R, Liu C, Yang C, Li Z, Xu D, Peng C, Jin Z, Xu C (2009) Rapid and sensitive detection of microcystin by immunosensor based on nuclear magnetic resonance. Biosens Bioelectron 25(1):240–243
27. Kristian N, Yan Y, Wang X (2008) Highly efficient submonolayer Pt-decorated Au nano-catalysts for formic acid oxidation. Chem Commun 3(3):353–355
28. Kristian N, Wang X (2008) Ptcore/C electrocatalyst with a controlled shell thickness and improved Pt utilization for fuel cell reactions. Electrochem Commun 10(1):12–15
29. Bruno MM, Franceschini EA, Planes GA, Corti HR (2010) Electrodeposited platinum catalysts over hierarchical carbon monolithic support. J Appl Electrochem 40(2):257–263
30. Tan F, Leung PHM, Liu ZB, Zhang Y, Xiao L, Ye W, Zhang X, Yi L, Yang M (2011) A PDMS microfluidic impedance immunosensor for E. coli O157:H7 and Staphylococcus aureus detection via antibody-immobilized nanoporous membrane. Sensors Actuators B Chem 159(1):328–335
31. Chen GZ, Yin ZZ, Lou JF (2014) Electrochemical immunoassay of Escherichia coli O157:H7 using Ag@SiO2 nanoparticles as labels. J Anal Methods Chem 2014(2):247034
32. Li Y, Cheng P, Gong J, Fang L, Deng J, Liang W, Zheng J (2012) Amperometric immunosensor for the detection of Escherichia coli O157:H7 in food specimens. Anal Biochem 421(1):227–233
33. Kawasaki S, Fratamico PM, Horikoshi N, Okada Y, Takeshita K, Sameshima T, Kawamoto S (2010) Multiplex real-time polymerase chain reaction assay for simultaneous detection and quantification of Salmonella species, Listeria monocytogenes, and Escherichia coli O157:H7 in ground pork samples. Foodborne Pathog. Dis 7(7):549–554
34. Zhang Y, Tan C, Fei R, Liu X, Zhou Y, Chen J, Chen H, Zhou R, Hu Y (2014) Sensitive chemiluminescence immunoassay for E. coli O157:H7 detection with signal dual-amplification using glucose oxidase and laccase. Anal Chem 86(2):1115–1122
35. Wu W, Zhang J, Zheng M, Zhong Y, Yang J, Zhao Y, Wu W, Ye W, Wen J, Wang Q (2012) Correction: an aptamer-based biosensor for colorimetric detection of Escherichia coli O157:H7. PLoS One 7(11):e48999
36. Jin S-A, Heo Y, Lin L-K, Deering AJ, Chiu GT-C, Allebach JP, Stanciu LA (2017) Gold decorated polystyrene particles for lateral flow immunodetection of Escherichia coli O157:H7. Microchim Acta 184(12):4879–4886. https://doi.org/10.1007/s00604-017-2524-5
37. Yang Z, Liu Y, Lei C, Sun XC, Zhou Y (2016) Ultrasensitive detection and quantification of E. coli O157:H7 using a giant magnetoimpedance sensor in an open-surface microfluidic cavity covered with an antibody-modified gold surface. Microchim Acta 183(6):1831–1837